Available online at www.sciencedirect.com

ScienceDirect

Procedia IUTAM 26 (2018) 153–161

Procedia IUTAM

www.elsevier.com/locate/procedia

IUTAM Symposium Wind Waves, 4–8 September 2017, London, UK

Laboratory study of temporal and spatial evolution of waves excited on water surface initially at rest by impulsive wind forcing

Lev Shemer

School of Mechanical Engineering, Tel-Aviv University, Ramat Aviv, Tel-Aviv 69978, Israel

Abstract

Evolution of waves excited by wind that varies in time is not yet understood sufficiently well. In the present study, waves generated from rest by an effectively impulsive wind forcing are studied in a small laboratory wind-wave tank. Multiple parameters characterizing evolution of the wave field in time as well as in space are presented. Measurements of the variation with time of the instantaneous surface elevation were performed simultaneously with determination of two components of the instantaneous surface slope at a number of fetches along the test section. For each wind forcing conditions, numerous independent realizations were recorded. Thus, sufficient data were collected for computation of statistically reliable ensemble-averaged values of parameters characterizing the evolving random wind-wave field as a function of time elapsed since the initiation of wind. In each realization, data acquisition started when the water surface was calm, and lasted until statistically steady random wave field conditions were attained. The analysis of the ensemble-averaged wind-wave characteristics indicated that distinct stages in the wind-waves evolution could be identified. These stages were compared with the predictions based on the viscous instability theory and on the random resonant wind-waves generation model.

Peer-review under responsibility of the scientific committee of the IUTAM Symposium Wind Waves.

Keywords: Generation of waves by wind; unsteady wind forcing; waves under wind gusts; Phillips wind-wave generation model; Kawai model

1. Introduction

The process of generation of sea waves by wind remains at the center of scientific interest for more than 150 years [1]-[3]. About 60 years ago, two different possible mechanisms of water-wave generation by wind were suggested: the resonant pressure fluctuations model by Phillips [4] and the shear-flow model by Miles [5]. Only very limited and not very successful attempts have been made so far to validate the Phillips model. The compilation by Plant [6] of experimental results on wind-waves growth rate from numerous studies exhibits significant scatter around the predictions by Miles theory. Miles [7] stressed that his model is inapplicable to the initial stages of wind-wave generation. Spatial growth rates at the steady wind forcing for fixed Fourier frequency harmonics were measured directly in the experimental facility used in the present study [8]; the results show behavior that is qualitatively inconsistent with the Miles predictions however fall into the domain of data scatter in the Plant [6] plot. Numerous studies [9]-[11] demonstrated that coupled viscous shear flow at the gas-liquid interface has a significant effect on the wave growth rates.

It should be stressed that while most of those theories assume unidirectional waves, the essentially three-dimensional structure of wind-wave field was emphasized in numerous experimental studies [12]-[14]. Moreover, the wind-wave generation theories mentioned above usually consider evolution of the wind-wave field in time (the duration-limited case), often assuming spatial homogeneity, whereas in the experiments the spatial (fetch-limited) evolution of waves due to effects of dispersion, wind input,

Peer-review under responsibility of the scientific committee of the IUTAM Symposium Wind Waves.
10.1016/j.piutam.2018.03.015

nonlinearity, and dissipation is measured. The wave field in this case may be statistically steady for steady wind forcing, but is spatially inhomogeneous.

Additional complexity of the problem of water waves' excitation by wind arises when wind forcing is unsteady, thus the statistical characteristics of waves that always depend on space now vary with time as well. Field experiments on wind waves under unsteady forcing are rare. Therefore, well-designed laboratory studies are needed that may provide detailed experimental data on wave evolution under controlled conditions needed for understanding the relative contribution of different mechanisms that govern the variation of the wind-wave field. However, even at laboratory scale only limited experimental data on waves under time-dependent wind under controlled conditions are currently available. Radars were used mostly in early studies of waves excited by impulsively started wind [15-16]. These data are restricted to waves with fixed lengths only defined by the Bragg resonance conditions.

First experimental and theoretical study of ripple excitation by abruptly started wind was carried out by Kawai [10] and provided evidence that viscous instability mechanism causes exponential growth of waves in time. Time-dependent results were often obtained by selecting short records and assuming quasi-steady conditions within each record. Veron & Melville [17] studied waves under slowly accelerating wind. The spectral information was obtained in this study assuming quasi-steadiness. Different techniques were applied in [18-19] to study wind stress under time-dependent wind, also effectively invoking the quasi-steady assumption.

The present paper is based on the experiments carried out by Zavadsky & Shemer [20] in a small wind-wave facility and presents time-resolved statistically reliable results on waves excited from rest by a (nearly) impulsive wind forcing. These experimental results are further discussed here. Different stages of wind-wave field evolution are delineated. Measurements were performed using multiple sensors and a fully automated experimental procedure. Running experiments without human intervention made it possible to carry out numerous independent realizations of temporally and spatially varying wave field under identical wind forcing conditions. The statistical wave parameters were computed at each fetch and wind forcing by averaging the data recorded for the accumulated ensemble of realizations as a function of time elapsed since the initiation of wind. The validity of different theoretical models is examined. Particular emphasis is given to the implications of nonexistence of spatial homogeneity on the evolution of the duration-limited wind-wave field.

2. Experimental facility and procedure

Experiments were carried out in a wind-wave facility that has a test section, which is 5 m long, 0.4 m wide and 0.5 m high. The test section is covered by removable transparent plates with a partially sealed slot along the centerline that facilitates positing of sensors. The test section is filled to water depth of about 0.2 m, thus deep-water conditions are satisfied for wind-waves with lengths pertinent to this study. Computer-controlled blower provides air flow rate with wind speed in the test section up to about 15 m/s. Instantaneous surface elevation was measured by a capacitance-type wave gauge made of 0.3 mm anodized tantalum wires and mounted on a computer-controlled vertical stage to enable its static calibration. The wind velocity in the test section, $U(t)$ was measured by a Pitot tube. Simultaneously with the surface elevation measurements, two components of the instantaneous surface slope, in the wind direction, $\partial\eta/\partial x$, and in the crosswind direction, $\partial\eta/\partial y$, were determined by a laser slope gauge (LSG). More details about the experimental facility and the instrumentation are given in [8] and [20]; for detailed description of the LSG set up and calibration procedure see [14].

Prior to activation of the blower in each experimental run, the water surface was calm. The blower output voltage represents the airflow rate; this voltage varies linearly at the rate of 1 V/s until the prescribed steady state is attained. The following set of the target wind velocities in the test section was used: U = 6.5 m/s, 7.5 m/s, 8.5 m/s, 9.5 m/s, and 10.5 m/s. Results of simultaneous measurements of the blower output voltage and of the wind velocity $U(t)$ as a function of time elapsed since the activation of the blower by the computer are presented in Fig. 1 for different target wind velocities. The duration of the ramp in the blower-driving signal varies from 3 s to 5 s. At each instant, the wind velocity lags slightly behind the blower output, the delay, however, does not exceed 1 s. Velocities below about 1.5 m/s are not measured adequately by the Pitot tube. Once the target velocity is attained, the blower maintains constant airflow rate in the test section for 120 s and is then shut down.

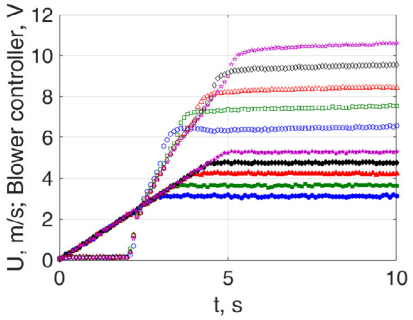

Fig. 1. Mean wind velocity (empty symbols) and the blower output voltage (filled symbols).

For all target wind velocities, turbulent airflow exists in the test section. The friction velocities at the air-water interface measured in our facility under steady forcing for a wide range of steady wind velocities were presented in [22]. Measurements were carried out at three distances from the inlet, at fetches x = 120 cm, 220 cm and 340 cm. The temporal variations of the instantaneous surface elevation η, of the surface slopes components $\partial\eta/\partial x$ and $\partial\eta/\partial y$, of the mean wind velocity $U(t)$, and of the voltage output were recorded at sampling frequency f_s = 300 Hz; data sampling started prior to activation of the blower.

Time interval between successive runs was set at about 6 min, sufficient for decay of all disturbances in the test section, so that at the initiation of the next run the water surface was calm again. The total duration of a single run, including the waiting period, thus exceeds 8 min. Usually at least 100 independent realizations for each set of operational parameters (the target wind velocity and the fetch) were recorded. The total duration of the experiments at a single fetch and wind target velocity thus exceeds 13 hrs. Measurements for all wind velocities at a single fetch, including wave gauge calibration for each wind velocity, last more than two days. Such long continuous experimental sessions and synchronization between the blower operation and data sampling are possible since the whole procedure, including operation of the blower, wave gauge calibration and data acquisition, is fully automated and controlled by a computer using a single LabView program, virtually without human intervention.

The accumulated set of data allows calculation of characteristic wave parameters ensemble-averaged for each fetch x and target wind velocity U over all realizations as a function of time elapsed relative to common reference taken as the instant of the blower initiation in each realization. The characteristic amplitudes of the surface elevation η and of the slope components $\partial\eta/\partial x$ and $\partial\eta/\partial y$ at each instant can be represented by their corresponding ensemble-averaged root-mean-square (r.m.s.) values calculated over the whole set of realizations relative to the reference. A different procedure was applied to determine the dominant wave frequency as a function of time elapsed since the blower activation. To this end, continuous real Morlet wavelet transform that decomposes a time-varying function into wavelets and offers good time and frequency localization was used. The wavelet 'spectrum', or map, was calculated for each realization; the resulting maps were then averaged over the whole set of realizations. The scale corresponding to the maximum intensity of the ensemble-averaged map defines the dominant pseudo-frequency at each instant.

3. Results and discussion

Under steady wind forcing, the wave field in the present experimental facility is essentially three-dimensional, as can be seen in the reconstruction of stereo video images as described in detail in [14]. Typical snapshot of the wave field is presented in Fig. 2.

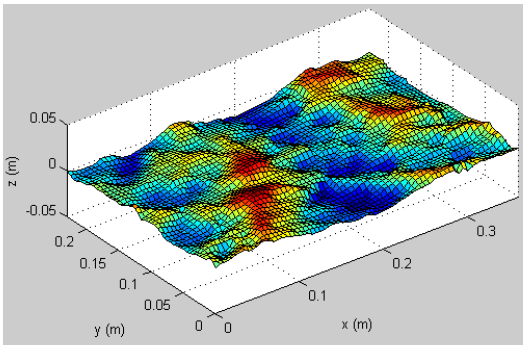

Fig. 2. Three-dimensional reconstruction of the instantaneous wind-wave field.
Steady wind velocity U =8.5 m/s; the centre of the image at x = 220 cm

An insight into the three-dimensional structure of the evolving in time wind-wave field can be obtained by examining the time variation of the simultaneously acquired surface elevation $\eta(t)$ and of both components of surface slope, $\partial\eta/\partial x(t)$ and $\partial\eta/\partial y(t)$, see Fig. 3. The records in this figure are scaled and shifted vertically for convenience.

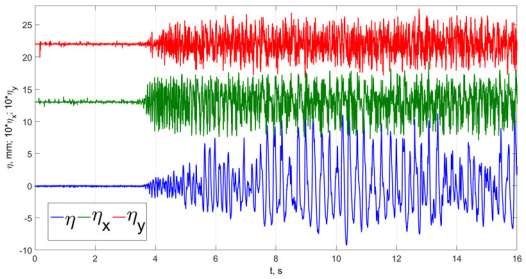

Fig. 3 Records of variation of the instantaneous surface elevation $\eta(t)$ and surface slope components, $\partial\eta/\partial x(t)$ and $\partial\eta/\partial y(t)$ under wind accelerated from rest to the target value U=8.5 m/s at fetch x=220 cm.

During the initial 3.5 s after the activation of the blower, there are no visible fluctuations of the surface elevation, η, as well as of the surface slope components. Comparison of figs. 2 and 3 demonstrates that it can be assumed that the wave field starts to develop only after the constant wind velocity in the test section has been attained, thus for target wind velocities $U \leq 8.5$ m/s, the wind forcing can effectively be presented by a step function. It takes about 9 s since the activation of the blower for the fluctuations of the surface elevation to attain the quasi steady-state; that is more than 5 s after the appearance of the initial visible disturbances at the water surface. The quasi-steady level of fluctuations of the surface slope component, $\partial\eta/\partial x$, however, is attained much faster, already at $t \approx 4$ s, just about 1 s after the inception of the first visible disturbances. The fluctuations of $\partial\eta/\partial y$ lag somewhat after the development of slopes in the wind direction, so that for a very short duration, less than 1 s, the wave field remains approximately unidirectional. Nevertheless, quasi-steady levels of slope fluctuations in both directions are attained at comparable times and notably earlier than that of η.

The main ensemble-averaged parameters are plotted for three fetches and three wind velocities as a function of the time elapsed from the activation of the blower in Fig. 4. The instantaneous r.m.s. values of the surface elevation, $<\eta^2>^{1/2}$, characterize the wave amplitude, while the values of $<(\partial\eta/\partial x)^2>^{1/2}$ serve as an indicator of the instantaneous wave steepness. Note that the behavior of $<(\partial\eta/\partial y)^2>^{1/2}$ is similar to that of $<(\partial\eta/\partial x)^2>^{1/2}$ and therefore not plotted

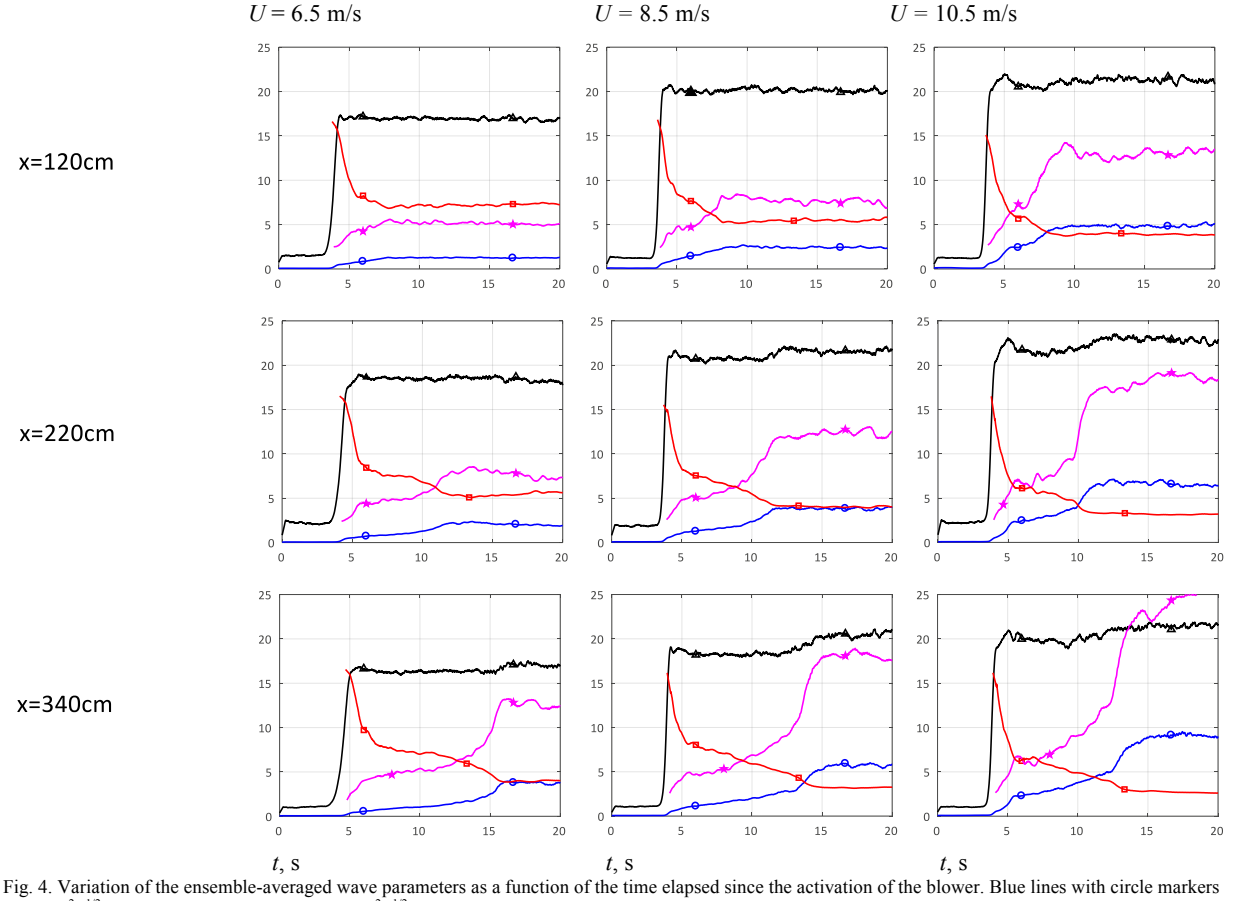

Fig. 4. Variation of the ensemble-averaged wave parameters as a function of the time elapsed since the activation of the blower. Blue lines with circle markers denote $<\eta^2>^{1/2}$, black lines with triangles - $<\partial\eta/\partial x^2>^{1/2}$, red lines with squares - dominant frequency f_d, magenta lines with pentagrams – dominant wavelength, λ_d.

In each panel of Fig. 4 the dominant frequency f_d and the corresponding wavelength, λ_d, are plotted as well. The dominant frequency f_d at each instant corresponds to the maximum scale of the ensemble-averaged wavelet map. The dominant wavelength is calculated for each f_d using the empirical dispersion relation obtained in the present experimental facility that accounts for the Doppler shift due to the induced current, see [8], [20].

All curves in Fig. 4 represent ensemble-averaged results with the temporal resolution of 3.3 ms. High temporal resolution enables distinguishing between stages in the wave field evolution. There are no essential disturbances at the water surface during the initial 4 s following the initiation of the blower at all fetches and wind velocities. During this period with no visible waves, the air velocity in the test section is accelerated to its final value, except for the highest flow rates employed in this study, see Fig. 1. Then, a rapid growth of very short waves with the r.m.s. values of surface elevation not exceeding approximately 1 mm is

observed along the whole length of the test section. This fast initial wave growth is accompanied by a nearly impulsive increase in the r.m.s. values of the characteristic surface slope $<(\partial\eta/\partial x)^2>^{1/2}$ up to the steady-state values that at a given wind velocity are nearly independent of fetch, x, and increase somewhat with U, varying in the range of 0.17 to about 0.22.

The initial ripples have characteristic frequency of f_d=15 Hz at least at all fetches and wind velocities. During the fast growth of the ripples, the values of f_d decrease. Also, for longer fetches and for higher target wind velocities, the characteristic frequencies are lower. Apparently, variation of the dominant wavelength, λ_d, is associated with that of f_d. Contrary to the fast variation of the surface slope components up to their steady-state value, the evolution of $<\eta^2>^{1/2}$, f_d and λ_d is much slower and at all fetches and wind velocities occurs at time scales that characterize the temporal variation of $<\eta^2>^{1/2}$. The time scales of the evolution increase with fetch and wind velocity.

Evolution in time of the characteristic wave amplitude, $<\eta^2>^{1/2}$, and of the characteristic instantaneous dominant frequency, f_d, are compared in Fig. 5 at two fetches x and for two values of the target wind velocity U. The comparison reveals that for each wind velocity U, at the instant when the instantaneous values of $<\eta^2>^{1/2}$ attain the value corresponding to the steady state at the shorter fetch, the corresponding dominant frequencies f_d also attain the steady state value at the shorter fetch. Similar results were obtained for other pairs of fetches and wind velocities considered in this study.

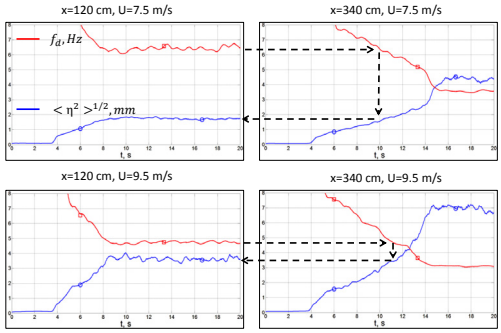

Fig. 5. Comparison of the variation with the elapsed time t of the ensemble-averaged wave amplitudes and the characteristic dominant frequencies at two fetches and two target wind velocities. The broken lines indicate the steady state values at the shorter fetch.

These observations fit within a conjecture that with the initiation of the blower over water at rest, a spatially homogeneous wave field is initially excited that contains a wide spectrum of harmonics. Under the action of wind, different frequency harmonics propagate with their respective group velocities c_g, grow in time and in space, until they attain equilibrium values of amplitude and steepness for the given steady wind forcing. Once a harmonic with the frequency f attains its equilibrium amplitude at a certain fetch $x(f)$, its amplitude remains constant and does not vary fast at longer fetches, $x > x(f)$. The duration of the growth stage at each fetch and wind velocity, $t_{gr}(x)$, can thus be estimated as the required propagation time

$$t_{gr} = x/c_g(f_d(x)) \tag{1}$$

This scenario implies that while short wind-waves are strongly nonlinear, their initial growth can be seen as an essentially linear process.

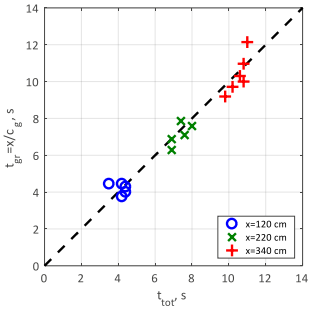

Fig. 6. The calculated according to the model duration of the initial wave growth process, t_{gr}, compared to the measured growth duration t_{tot}.

The values of the total durations of the growth stage, t_{gr}, calculated using the suggested relation, and the empirical values of group velocity for each dominant wavenumber, are compared in Fig. 6 with the actual duration of the growth stage t_{tot} estimated from the experimental data presented in Fig. 4. Note that the initial reference point is taken at the instant when blower capacity attains maximum, *i.e.* 3.5–5.5 s after the activation of the blower, depending on the target value of U, see Fig. 1. Fig. 6 demonstrates that good agreement between these values is obtained for all fetches and wind velocities.

It can clearly be seen in Fig. 4 that there are notable changes of the slopes of the curves representing the temporal variation of the measured parameters that occur essentially simultaneously for all those parameters and suggest division of the temporal

evolution of the wave field into distinct stages. To define those stages, the variation with the elapsed time of the characteristic instantaneous wave amplitude, $<\eta^2>^{1/2}$, is plotted in Fig. 7 for x=340 cm and the target wind velocity U=7.5 m/s.

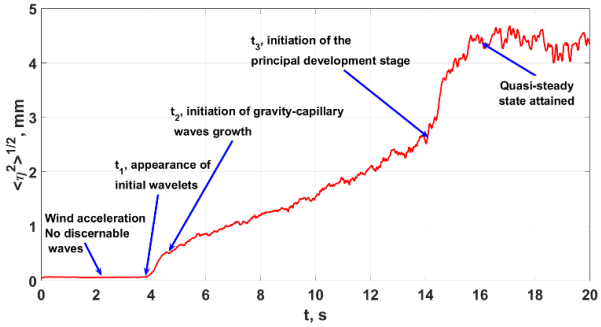

Fig. 7. Definition of characteristic times in temporal variation of the representative wave amplitude (x = 340 cm, U = 7.5 m/s)

When the first wavelets become detectable at the elapsed time t_1, the wind velocity has already attained its target value, see Fig. 1. The fast initial growth of these short ripples decreases abruptly at t=t_2. Note that at t_2, the characteristic wave amplitudes are still less than 0.5 mm, however, the representative wave steepnesses already attain their limit values (*cf.* Fig. 4). The significantly slower wave growth continues for t_2<t<t_3; then at t_3 the rate of wave amplitude growth accelerates, until the temporal wave evolution process ceases at t_4 that in fact corresponds to the total duration of the wave growth at the prescribed location and wind velocity denoted in Fig. 6 as t_{tot}.

The distinct stages in the wind-wave evolution with the elapsed time t identified in Fig. 7 suggest that at each stage, a different mechanism governs the wave growth. Therefore, the temporal evolution of wind-waves is now analyzed separately for at each stage. An attempt is made to relate the experimental results to the existing theoretical models.

In view of delay in the initial response of the water surface to the activation of the blower, for lower target wind velocities, the forcing is effectively impulsive, see Fig. 1. The initial growth of ripples excited by such an impulsive wind forcing is plotted in Fig. 8. Plot in semi-logarithmic coordinates demonstrates that the growth with time of the energy $<\eta^2>$ of the initial ripples is exponential and thus can be approximated as

$$\langle \eta^2(t) \rangle = \langle \eta_0^2 \rangle e^{\beta t} \tag{2}$$

where $\langle \eta_0^2 \rangle$ is the initial disturbance energy and β the growth parameter. The values of β for different target velocities (including those not presented in Fig. 8 are summarized in Table 1.

Table 1. Initial ripples growth parameter β (s^{-1}).

Fetch (cm)	U=6.5 m/s	U=7.5 m/s	U=9.5 m/s	U=10.5 m/s
120	7.6	12.0	11.7	12.2
220	7.1	9.4	12.0	13.9
340	5.9	7.8	10.0	10.7

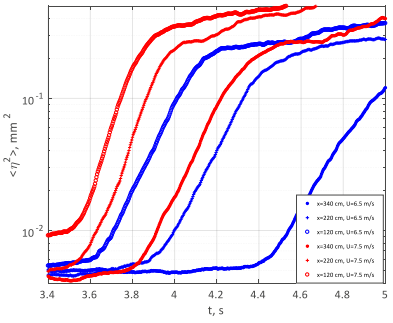

Fig. 8. Exponential growth of the energy of initial ripples for lower target wind velocities U.

As can be seen in Fig. 8, the duration of the exponential growth is only about 200-300 ms. Sufficiently high sampling rates are therefore needed for unambiguous determination of the growth parameter β (3oo Hz were used in this study). The exponential growth of wavelets in Fig. 8 may be attributed to linear instability mechanism that becomes essential at instant t_1, see Fig. 7. Note that for a given target wind velocity U, the growth rate parameter β decreases with fetch. The growth rate parameters β given in Table 1 compare favorably with the computations and the experimental results reported by Kawai [10]. Due to different forcing

conditions in the present study as compared to those in [10], extrapolation of the results of [10] to stronger wind forcing was carried out in this comparison.

Termination of the exponential growth stage of the initial ripples can plausibly be attributed to significant wave nonlinearity characterized in Fig. 4 by the instantaneous representative steepness $<(\partial\eta/\partial x)^2>^{1/2}$ that attain their maximum quasi-steady values at times close to the ending of the exponential growth stage. However, an additional factor may be considered that renders the application of the linear viscous instability theory of unidirectional waves inapplicable at $t>t_2$. Single realization records presented in Fig. 3 suggest that the growth of $\eta_x = <(\partial\eta/\partial x)^2>^{1/2}$ precedes that of $\eta_y = <(\partial\eta/\partial y)^2>^{1/2}$. In Fig. 9, the variation with the elapsed time of these two parameters is plotted during the initial evolution stages for the conditions corresponding to Fig. 7. The slopes in the crosswind direction, y, grow notably slower than those in the wind direction, x, and attain their quasi-steady-state values later. The initial wavelets that grow exponentially are therefore largely unidirectional, in accordance with the assumptions adopted in [10].

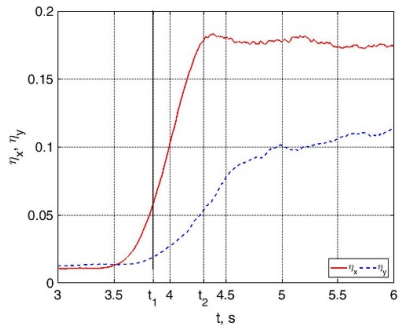

Fig. 9. The initial growth of the r.m.s. values of the ensemble averaged instantaneous slope components $\eta_{x \text{ and }} \eta_y$. Vertical lines denote characteristic times t_1 and t_2 defined in Fig. 7.

The Phillips [4] theory can be applied to describe wave evolution following the appearance of the initial ripples, $t>t_2$. The theory suggests two-stage temporal evolution of wind-waves due random pressure fluctuations. In our experiments, the 'initial growth stage' according to Phillips may be attributed to elapsed times $t_2<t<t_3$. There is no closed expression predicting the wind–wave growth at this stage in [4]; rather, the theory states that the mean values of $<\eta^2>$ initially grow linearly with time. The measured dependence of the mean wave energy $<\eta^2>$ on the elapsed time is therefore plotted in Fig. 10 as a function of $(t - t_2)$. In spite of a considerable scatter in the data, particularly at higher target wind velocities U, the wave energy indeed seems to increases notably on the fetch x. The initial growth stage becomes shorter as the target wind velocity U increases.

At $t = t_3$, the wave energy growth becomes notably faster. The wind–wave field evolution at $t>t_3$ may be associated with 'the principal stage' in the Phillips [4] theory, this stage terminates when the quasi-steady is attained at each fetch and wind velocity at $t \approx t_4$. It can be seen in Fig. 4 that waves observed in our facility at fetches x = 220 cm and x = 340 cm have lengths exceeding 7 cm and thus can be considered as purely gravity waves practically unaffected by capillarity.

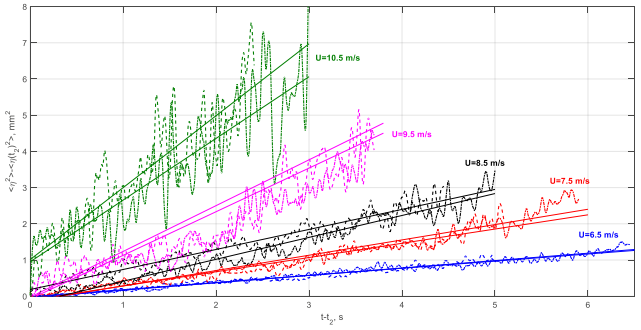

Fig. 10. The temporal growth of wind waves associated with Phillips 'initial growth stage'. Dashed lines correspond to the fetch x=220 cm, dash-dot lines to fetch x=340 cm; solid lines – linear fits.

For temporal growth of gravity waves at the principal stage of development, Phillips obtained the following relation:

$$\overline{\eta^2} \sim \frac{\overline{p^2}t}{2\sqrt{2}\rho_w^2 U_c g} \tag{3}$$

In (3), $\overline{p^2}$ represents mean square pressure fluctuations at the surface, U_c is the convection velocity of those fluctuations that are assumed in [4] to correspond to the phase velocity of water waves, while ρ_w is the water density. It is further assumed that the turbulent pressure fluctuations are related to interfacial shear stress, $\tau = \rho_a u_*^2$, where u_* is the friction velocity at air–water interface, so that $\overline{p^2} \sim u_*^4$. It is also assumed in [4] that the convection velocity of the pressure fluctuations is related to the friction velocity: $U_c = 18u_*$. The relation (3) is thus rewritten as

$$\overline{\eta^2} \sim 0.035 \left(\frac{\rho_a}{\rho_w}\right)^2 \frac{U^3 t}{g} \tag{4}$$

Thus, according to the theory of Phillips the wave energy of short gravity waves grows linearly with time, while the growth rate is proportional to the cube of wind velocity. However, the characteristic wave velocity for short gravity waves (10 cm < λ < 30 cm) measured in the present experimental facility [20] is in fact nearly constant and remains substantially lower than the wind velocity, being essentially independent of U. These observations prompted us to approximate the convection velocity U_c by a constant value for the conditions of the present experiments. By incorporating this assumption into (3), the relation (4) is replaced by

$$\langle \eta^2 \rangle = C U^4 t. \tag{5}$$

In (5), the dimensional coefficient C is supposed to be constant in the framework of Phillips approach.

To examine the validity of (5), the measured variation of $\langle \eta^2 \rangle / U^4$ is plotted in Fig. 11 as a function of time elapsed since the initiation of the principal stage of wind–wave development, $t = t_3$. The results are given for two fetches (x = 220 cm and x=340 cm) and three wind velocities U = 8:5 m/s, U= 9.5 m/s and U=10.5 m/s. All dependencies are well approximated by straight lines thus confirming linear growth of the wave energy with time during this stage as well. The nearly identical slopes are obtained for different wind velocities for the longer fetch, x=340 cm. For the shorter fetch, x=220 cm, the slopes are similar but differ somewhat, with no identifiable trend of the slope dependence on the wind velocity U. All slopes in Fig. 11 are of the same order, in general agreement with the relation $\langle \eta^2 \rangle \sim U^4$.

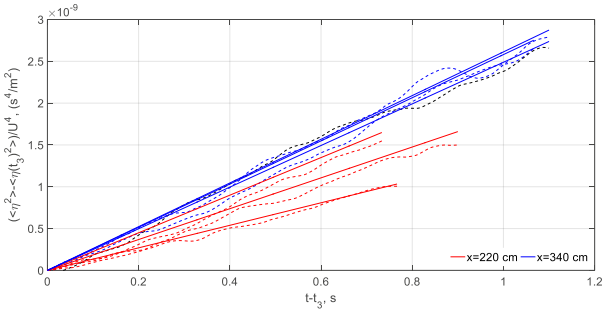

Fig. 11. Variation with time of $\langle \eta^2 \rangle / U^4$ during the 'principal development stage' of Phillips.

Evolution of waves under impulsive wind forcing can thus be characterized by distinct stages. First, initial wavelets appear nearly simultaneously in the whole test section. These wavelets are effectively two-dimensional and their energy grows exponentially with time, thus providing experimental validation of applicability of deterministic 2D viscous instability mechanism [9, 10]. The duration of the exponential growth stage, however, is very short and does not exceed 1 s. The waves at the end of the exponential growth stage are quite steep; however, their height does not exceed about 1 mm. These results on the initial temporal growth are in agreement with the spatial evolution pattern of ripples under steady wind forcing [13]. Following the termination of the exponential growth stage, the wave field becomes essentially random and three-dimensional, see Figs. 3, 9, additional evidence to this effect is presented in [20]. Transition of the wave field from quasi-deterministic and two-dimensional to random and three-dimensional at $t \approx t_2$ results in growth of wind waves at later stages that is qualitatively different. With termination of the exponential growth stage, the wave energy at all fetches and for all target wind-velocities increases essentially linearly with time, see Fig. 10, while the dominant wave frequency continues to decrease, albeit more slowly.

It should be noted that linear with time growth of disturbances under random forcing is quite common in diverse physical systems. For water waves, the linear growth in time was suggested first by Phillips [4] as his 'initial development stage'. More recently, Milewski et al. [23] demonstrated theoretically that the energy of nonlinear wave systems under random forcing with negligible dissipation grows linearly with time. At longer times, $t > t_3$, the wave energy continues to grow linearly with time until the quasi-steady state is attained, but the growth rate increases notably. The wave energy variation at this later evolution stage may be loosely attributed to the Phillips [4] resonant mechanism that becomes dominant, causing linear in time, but notably faster growth; this wave energy growth may be related to the 'principal stage of development' in his theory.

4. Conclusions

Large ensembles of independent experimental runs starting from rest were recorded at sufficiently high sampling frequency for several fetches and target wind velocities. These data enabled computation of variation of wave parameters averaged over the accumulated ensembles of data as a function of time elapsed since the initiation of the blower. The results allow identifying distinct stages of wave field evolution in time under effectively impulsive wind forcing.

Although waves in the present experiments becomes steep very fast and thus essentially nonlinear, variation of the dominant wave frequency and of the characteristic wave amplitude with fetch for a given target wind velocity can be described fairly well by a scenario based on an essentially linear approach.

The initial growth of short ripples measured in the present study is exponential in time. The growth rate is consistent with the prediction based on viscous instability theory [10]. However, the exponential stage of the wave growth lasts for a fraction of a second, and terminates once the wave field becomes strongly nonlinear and essentially three-dimensional, while the characteristic wave heights remain small. It should be stressed that generalizations of the Miles [5, 7] model that take into account viscosity [9, 10] retain the linear, deterministic and two-dimensional approach adopted by Miles.

All those assumptions cease to be valid at the end of the exponential evolution stage. The nonlinearity of the wind wave field in the present experiments cannot be neglected anymore; moreover, waves lose their coherence and become random and three-dimensional. Linear deterministic approach thus fails to explain later evolution stages. An attempt is made here to describe the behavior of wind-waves during the subsequent growth invoking the theory suggested by Phillips for random wind forcing that is free of assumptions of linearity and two-dimensionality.

The present results clearly demonstrate that the temporal evolution of waves on an initially smooth water surface under impulsive wind forcing is inhomogeneous and strongly dependent on fetch. Thus, an approach in which spatially uniform wave field evolves in time only, is physically unrealistic. Temporal evolution of a wave field due to wind input, dissipation and/or nonlinearity is necessarily accompanied by spatial variations. The validity of theoretical and numerical results based on application of spatially periodic boundary conditions thus has to be carefully verified in experiments.

Acknowledgements

Support of this research by the Israel Science Foundation (grant no. 306/15) is gratefully acknowledged.

References

1 H. von Helmholtz, Über discontinuirliche Flüssigkeits-Bewegungen, *Akademie der Wissenschaften zu Berlin*, 1868.
2 Lord Kelvin, Hydrokinetic solutions and observations, *Philosophical Magazine*, 1871, 42: 362–377.
3 H. Jeffreys, On the formation of water waves by wind, *Proceeding of the Royal Society London, Ser. A*, 1925, 107: 189–206.
4 O. M. Phillips, On the generation of waves by turbulent wind, *Journal of Fluid Mechanics*, 1957, 2, 417–445.
5 J. W. Miles, J. W. On the generation of surface waves by shear flows, *Journal of Fluid Mechanics*, 1957, 3: 185–204.
6 W. J. Plant, A relationship between wind stress and wave slope, *Journal of Geophysical Research*, 1982, 87: 1961–1967.
7 J. W. Miles, Surface-wave generation revisited, *Journal of Fluid Mechanics*, 1993, 256: 427–441.
8 D. Liberzon, L. Shemer, Experimental study of the initial stages of wind waves' spatial evolution, *Journal of Fluid Mechanics*, 2011, 681: 462–498.
9 G. R. Valenzuela, 1976 The growth of gravity-capillary waves in a coupled shear flow, *Journal of Fluid Mechanics* 1976, 76: 229-250.
10 S. Kawai, Generation of initial wavelets by instability of a coupled shear flow and their evolution to wind waves, *Journal of Fluid Mechanics,* 1979, 93: 661-703.
11 K. van Gastel, K., P. A. E. M. Janssen, G. J. Komen, 1985 On phase velocity and growth rate of wind-induced gravity-capillary waves, *Journal of Fluid Mechanics,* 1985, 161: 199-216.
12 G. Caulliez, G. F. Collard, Three-dimensional evolution of wind waves from gravity-capillary to short gravity range, *European Journal of Mechanics, B/Fluids*, 1999, 18: 389–402.
13 G. Caulliez, N. Ricci, R. Dupon, The generation of the first visible wind waves, *Physics of Fluids,* 1998, 4: 757-759.
14 A. Zavadsky, A. Benetazzo, L. Shemer, L., On the two-dimensional structure of short gravity waves in a wind wave tank, *Physics of Fluids*, 2017, 29, 016601.
15 T. R. Larson, J. W. Wright, Wind-generated gravity-capillary waves: laboratory measurements of temporal growth rates using microwave backscatter. *Journal of Fluid Mechanics*, 70, 1975: 417–436.
16 W. J. Plant, J. W. Wright, Growth and equilibrium of short gravity waves in a wind–wave tank, *Journal of Fluid Mechanics*, 1977, 82: 767–793
17 F. Veron, W. K. Melville, Experiments on the stability and transition of wind-driven water surfaces, *Journal of Fluid Mechanics,* 2001, 446: 25–65.
18 B. M. Uz, M. A. Donelan, T. Hara, E. J. Bock, Laboratory studies of wind stress over surface waves. *Boundary-Layer Meteorology*, 2002, 102: 301–331.
19 B. M. Uz, T. Hara, E. J. Bock, M. A. Donelan, Laboratory observations of gravity capillary waves under transient wind forcing, *Journal of Geophysical Research,* 2003*,* 108: 3050.
20 A. Zavadsky, L. Shemer, Water waves excited by near-impulsive wind forcing, *Journal of Fluid Mechanics, 2017,* 828: 459-495.
21 A. Zavadsky, D. Liberzon, L. Shemer, Statistical analysis of the spatial evolution of the stationary wind wave field, *Journal of Physical Oceanography,* 2013, 43: 65-79.
22 A. Zavadsky, L. Shemer, Characterization of turbulent air flow over evolving water-waves in a wind wave tank, *Journal of Geophysical Research,* 2012, 117: C00J19.
23 P. A. Milewski, E. G. Tabak, E. Vanden-Eijnden, Resonant wave interaction with random forcing and dissipation. *Studies in Applied Mathematics*, 2002, 108: 123–144.